Synchronized Stimulation and Continuous Insulin Sensing in a Microfluidic Human Islet on a Chip Designed for Scalable Manufacturing

Aaron L. Glieberman, Benjamin D. Pope, John F. Zimmerman, Qihan Liu, John P. Ferrier Jr., Jennifer H. R. Kenty, Adrian M. Schrell, Nikita Mukhitov, Kevin L. Shores, Adrian Buganza Tepole, Douglas A. Melton, Michael G. Roper and Kevin Kit Parker

Supplementary Information

Supplementary Tables

Table S1 | Modeling Parameters

	Property	Variable	Value
Physical properties	Liquid	-	Water
	Temperature of fluid	T	310.15 K
	Dynamic viscosity	μ	6.913E-4 Pa*s
	Boltzman constant	k_b	1.381E-23 J/K
Islet properties	Islet diameter	d_{islet}	200, 250 μm
	Islet porosity	ε_{islet}	0.1
	Islet permeability	κ_{islet}	1e-15 m^2
Channel dimensions	Channel width	w	0.4 mm
	Channel height	h	0.4 mm
	Shunt length	L_{shunt}	278 mm
	Glucose mixing channel length	$L_{mixing,glu}$	22 mm
	FITC-Insulin mixing channel length	$L_{mixing,FITC}$	56 mm
	Insulin antibody mixing channel length	$L_{mixing,Ab}$	160 mm
Flow conditions	Trap flow rate	Q_{trap}	0.1 μl/min
	Islet inlet flow rate	Q_{ins}	0-1.4 μl/min
	Glucose inlet flow rate	Q_{glu}	0-1.4 μl/min
	FITC inlet flow rate	Q_{FITC}	0.1 μl/min
	Antibody inlet flow rate	Q_{ab}	0.1 μl/min
	Outlet pressure	P_{out}	0 Pa (gauge)
Diffusion conditions	Low glucose concentration	$c_{gluc,low}$	2.8 mM
	High glucose concentration	$c_{gluc,high}$	20 mM
	Insulin concentration	c_{ins}	75 mIU/mL *
	Glucose diffusivity in media	D_{glu}	4.0e-10 m^2/s [31]
	Insulin molecular radius	r_{ins}	1.34 nm [32]
	Insulin diffusivity in media	D_{ins}	11.6e-11 m^2/s [32]
	Fluorescein molecular radius	r_{ins}	0.55 nm [34]
	FITC-Insulin diffusivity in media	D_{FITC}	10.9e-11 m^2/s
	IgG molecular radius	r_{Ab}	5.5 nm [33]
	Insulin antibody diffusivity in media	D_{ab}	2.83e-11 m^2/s

* 1 nM Insulin = 167 μIU.

Table S2 | Human Islet Donor Information

Donor	Gender	Age	BMI	HbA1c (%)
1	F	46	19.0	5.8
2	M	61	28.8	5.1
3	M	66	27.0	4.7
4	M	34	28.0	5.2
5	F	62	30.1	5.2
6*	F	59	24.7	5.3

* Insulin secretion measured in Figure 7c

Supplementary Movies

Movie S1 | Automatic capture of human islets on chip.

Movie S2 | Parallel delivery of 10-minute fluorescent glucose pulse to human islets on chip.

Supplementary Figures

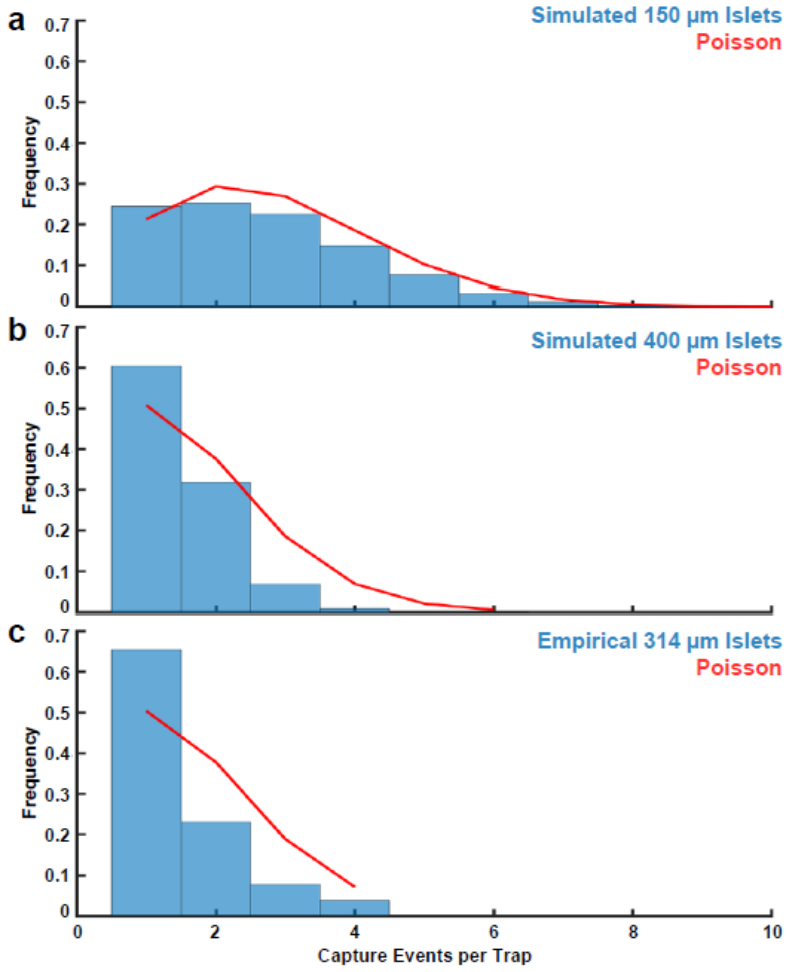

Figure S1 | Simulated and empirical distributions of islet capture events on the Islet on a Chip. a. Histogram (blue) of the number of 150 µm diameter islets captured per trap in 10,000 simulated loading experiments. A zero truncated Poisson distribution with the same mean (2.8 islets per trap) as the simulated data is also shown (red). A significant difference (p = 1.1 x 10^{-16}; Chi-square Goodness of Fit test) between Poisson and simulated distributions was observed. **b.** Histogram (blue) of the number of 400 µm diameter islets captured per trap in 10,000 simulated loading experiments. A zero truncated Poisson distribution with the same mean (1.5 islets per trap) as the simulated data is also shown (red). The difference between Poisson and simulated distributions for 400 µm diameter islets was significant (p = 1.1 x 10^{-16}; Chi-square Goodness of Fit test) and larger than for 150 µm diameter islets (D = .174 versus D = .057; Kolmogorov-Smirnov statistic). Simulated distributions also differed significantly for islets diameters of 150 and 400 µm (p = 1.1 x 10^{-16}; D = .426; two-sample Kolmogorov-Smirnov test). **c.** Histogram (blue) of the number of capture events per trap in two empirical loading experiments. On average, islets or islet clusters were 314 µm in diameter. A zero truncated Poisson distribution with the same mean (1.5 capture events per trap) as the empirical data is also shown (red). For our sample size (n = 39 capture events in 26 traps observed live for two separate experiments), the empirical distribution did not differ significantly from either the Poisson (p = .08; Chi-square Goodness of Fit test) or simulated distributions for 400 µm diameter islets (p = .99; D = .049; two-sample Kolmogorov-Smirnov test), but was more similar with the simulated distribution (D = .049 versus D = .223; Kolmogorov-Smirnov statistic). Differences relative to Poisson distributions are due to increased likelihood of traps with a single capture event and decreased likelihood of all other cases. The increased likelihood of a single capture event per trap is attributable to increased flow resistance in occupied relative to unoccupied traps and indicates an influence of trapping events on one another. This influence violates an assumption of Poisson distributions that events occur independently. Based on these results we conclude our loading simulations, which account for the interdependence of trapping events, are more appropriate for modeling islet loading on our chip than Poisson distributions.

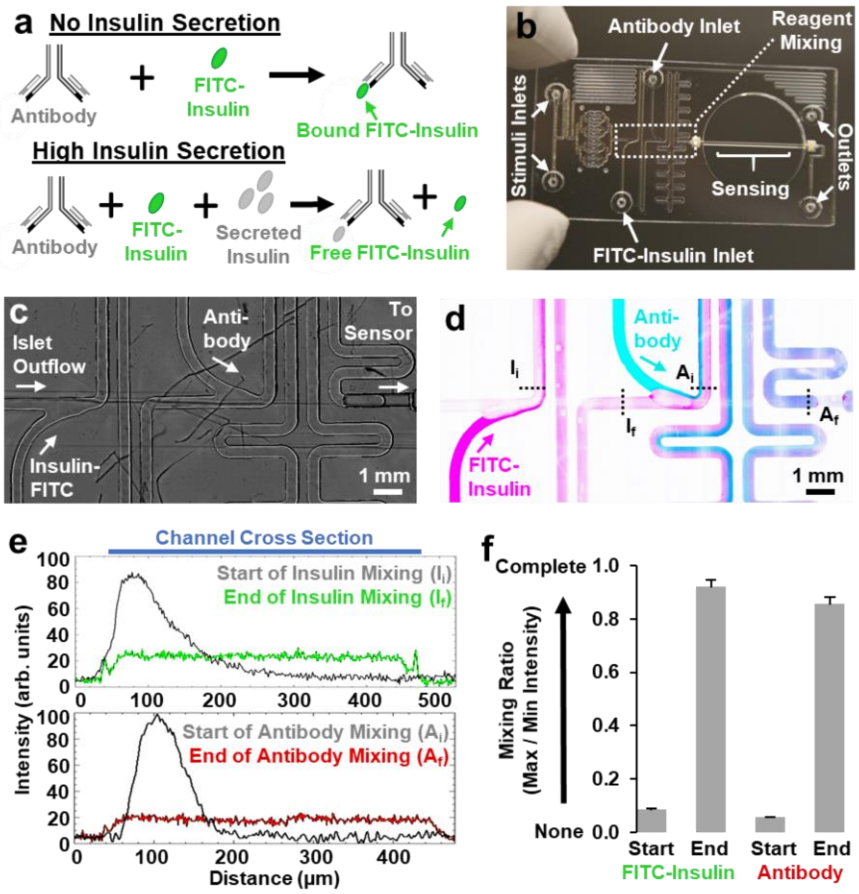

Figure S2 | Insulin immunoassay in the Islet on a Chip. a. Illustration of the competitive insulin immunoassay principle. Fixed amounts of exogenous, fluorescently labeled insulin (green oval, FITC-insulin) compete with secreted insulin (gray ovals) for binding to a limiting insulin antibody (gray Y). The fraction of FITC-insulin bound by the antibody is inversely proportional to the amount of insulin secreted. **b.** Photograph of the chip with a white, dotted box indicating the region where immunoassay reagents are introduced and mixed. **c.** Optical micrograph of the region where immunoassay reagents are introduced and mixed. **d.** Fluorescent micrograph of the region in panel c showing the introduction of FITC-insulin (pink) and a secondary antibody (blue) into the outflow from the islet trap region. Contrast was inverted for visualization. **e.** Signal intensities across the channel is shown at indicated points. **f.** Quantification of mixing at the start and end of the FITC-insulin (green) and antibody (red) channels.

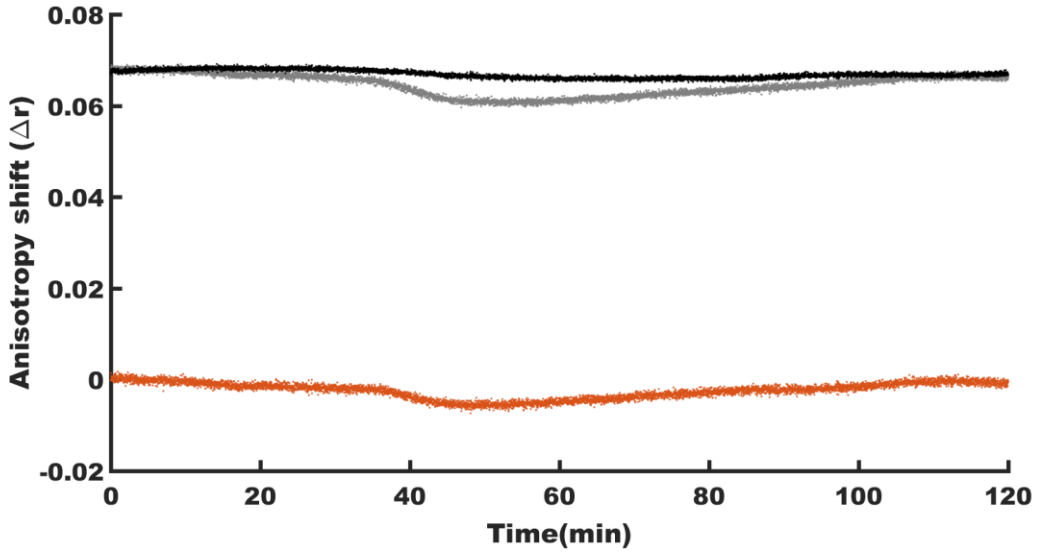

Figure S3 | Glucose dependent fluorescence anisotropy shift correction. Plot shows the normalized trace (orange) used for insulin secretion quantification that is obtained when a background recording of fluorescence anisotropy from alternating low (2.8 mM) and high (20 mM) glucose levels introduced to the chip without cells (black) is subtracted from the trace recorded when the same conditions are delivered to cells (grey).

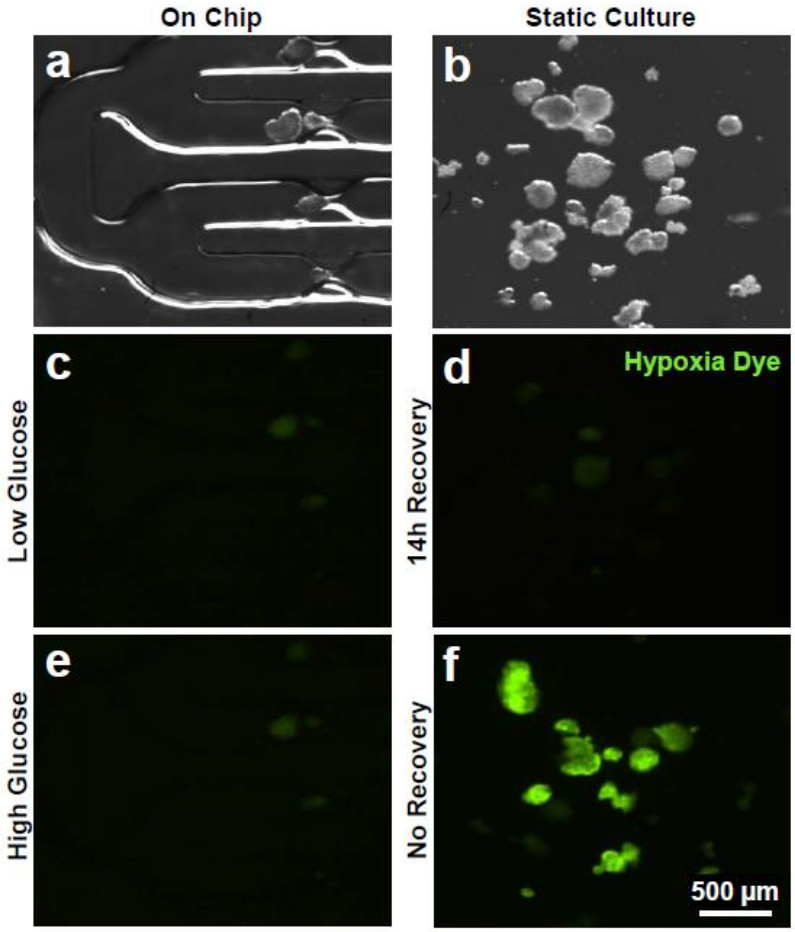

Figure S4 | On-chip perifusion and glucose stimulation does not induce hypoxia in human islets. a-b. Phase contrast micrographs of islets in low glucose media on the chip or in static culture. **c-d.** Fluorescence micrographs of the fields of view shown in a-b. Islets were allowed to recover from shipping for 14 hours in culture and then pretreated with dye that generates a green fluorescent metabolite under hypoxic conditions. **e.** The same field of view as in panel following a 70-minute pulse of high glucose. **f.** Islets treated with hypoxia dye immediately after shipping was a positive control for hypoxia. Scale bars are 500 µm.

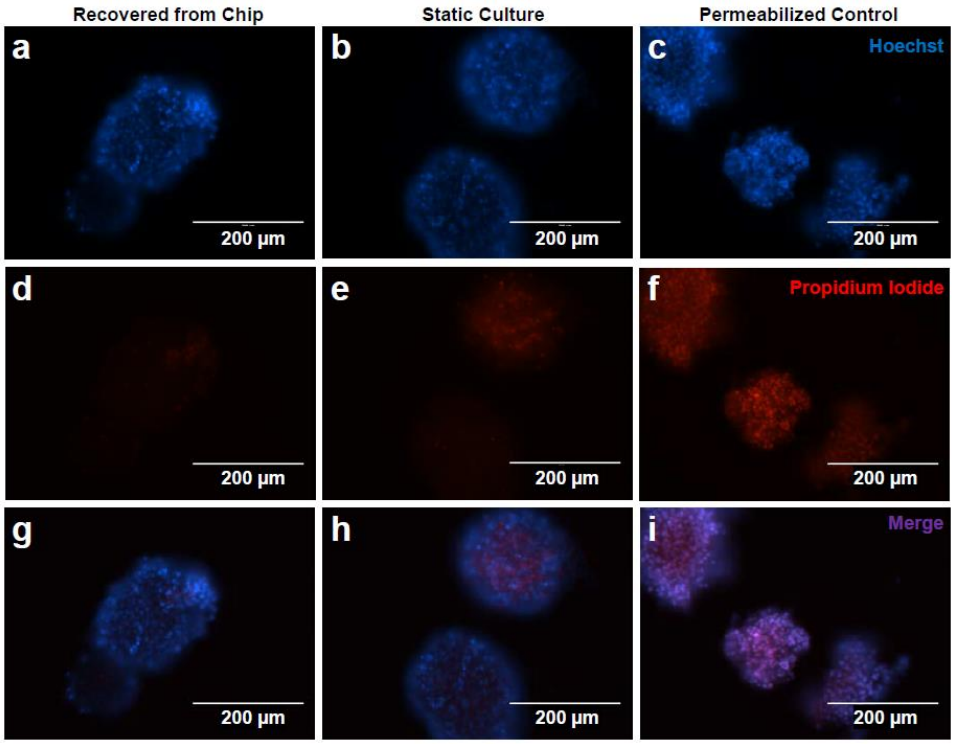

Figure S5 | Human islets survive collection after on-chip glucose stimulation. a-c. Fluorescence micrographs of nuclei within human islets that were either removed from the chip after a 70-minute on-chip glucose stimulation or maintained in static culture. Nuclei were stained with live-cell permeable Hoechst stain. **d-f.** Nuclei within dead cells were also stained with live-cell impermeable propidium iodide. Islets permeabilized with detergent served as a positive control for propidium iodide staining. **g-i.** Merged Hoechst and propidium iodide channels are also shown. Scale bars are 200 µm.